Supporting Information

Naphthalene Diimide Ammonium Directed Single-Crystalline Perovskites with 'Atypical' Ambipolar Charge Transport Signatures in Two-Dimensional Limit

Xiaomin Li,[1] Jin Yang,[2] Ziyi Song,[3] Ruiping Chen,[4] Lulu Ma,[5] Haining Li,[1] Jiong Jia,[1] Jiao Meng,[1] Xuan Li,[1] Mingdong Yi,[3] Xuan Sun[1,*]

[1]Key Laboratory for Colloid & Interface Chemistry, Shandong University, Ministry of Education, Jinan, 250100, P. R. China
[2]School of Microelectronics, Shandong University, Jinan, 250100, P. R. China
[3]Key Laboratory for Organic Electronics & Information Displays (KLOEID) and Institute of Advanced Materials (IAM), Nanjing University of Posts Telecommunications, Nanjing 210023, P. R. China
[4]State Key Lab of Structural Chemistry, Fujian Institute of Research on the Structure of Matter, Chinese Academy of Sciences, Fuzhou, 350002, P. R. China
[5]School of Material Science and Engineering, Shandong Provincial Key Laboratory of Preparation and Measurement of Building Materials, University of Jinan, 250022, P. R. China
*Corresponding author: email: sunxuan@sdu.edu.cn

Content

1. Experimental section: Synthesis and characterization

1.1.Instruments and measurements.

^{1}H NMR spectra were recorded on a Bruker 300 MHz NMR spectrometer. The room temperature UV-Vis absorption spectra were recorded on Agilent Cary Series UV-Vis spectrophotometer. Scanning electron microscopy (SEM) was obtained with a SU8010 field emission scanning electron microscope. Mapping was recorded on a Bruker XFlash 6l60. Powder X-ray diffraction (PXRD) was measured by Rigaku D/max-γB X-ray diffractomete. Atomic force microscopy (AFM) observations were carried out on a Dimension Icon (American) equipped with a SCANASYST-AIR silicon nitride probe with scan asyst.

1.2. Synthetic procedure.

1.2.1. Synthesis of compound NDIA

Scheme S1. Synthetic procedure of the asymmetric naphthalene diimide ammonium NDIA.

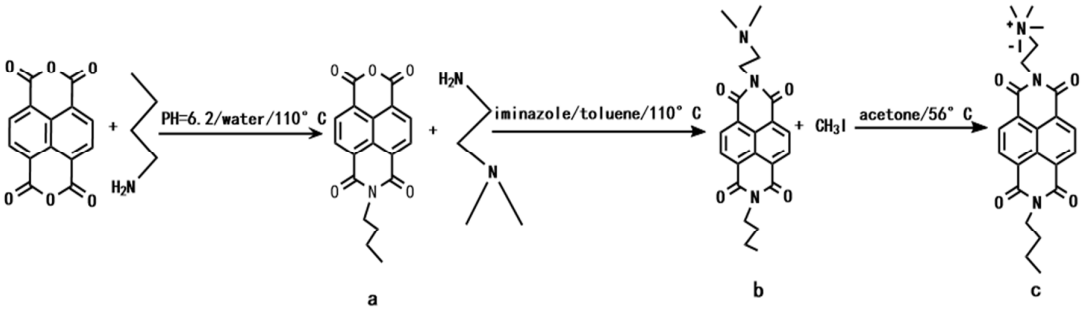

7-butyl-1,3,6,8-tetrahydro-1H-isochromeno[6,5,4-def]isoquinolin-5-ylium (a)[S1]

1,4,5,8-naphthalene-tetracarboxylic dianhydride (NTCDA, 0.4g, 1.49 mmol) was dispersed into 60 mL water. 7.5 mmol potassium hydroxide were dissolved in 5mL water, they were mixed and stirred until dissolved. The PH value is adjusted close to 6 with 1mol/L H_3PO_4 aqueous solution. Then 1.5 mmol n-Butylamine were added to the mixture, which was stirred at 110 °C for 12h. The solution was cooled down to room temperature. Hydrochloric acid (2mol/L) was added to adjust PH until the appearance of precipitation. The precipitation was washed several times with water and dried. Crude product was dissolved in acetic anhydride at 110℃ with stirring under a nitrogen atmosphere. Then the acetic anhydride was removed in vacuum and the n-butylamine substituted asymmetric naphthalene (**a)** was obtained with the yield of 63.3% (0.3527g). ^{1}H NMR (300 MHz, DMSO): δ 8.687 (*s*, 4H), 4.061 (t, *J* = 7.5Hz, 2H), 1.646 (m, *J* = 7.5Hz, 2H), 1.391 (m, *J* = 7.38, 2H), 0.936 (t, *J* = 7.2, 3H).

7-butyl-2-(2-(dimethylamino)ethyl)-1,3,6,8-tetraoxo1,2,3,6,7,8-hexahydrobenzo[lmn][3,8]phenantheolin-4-ylium (b)[S1]

N,N-Dimethyl-1,2-ethanediamine (0.1056g, 1.2 mmol), **a** (0.323g, 1 mmol), and imidazole (1g) were dissolved in 120 mL distilled toluene, then refluxed at 110 ºC for 24h under the protection of N_2. Then the solvent was removed in vacuum. The solid was dissolved with CH_2Cl_2, and then washed with water for three times to remove the imidazole. The organic layer was dried and evaporated in vacuum to afford the yellow solid. The crude product was purified by chromatography with eluent of CH_2Cl_2/CH_3OH, 100:7 v/v. The product with yellow color and yield of 33% (0.1305 g) was finally obtained. ^{1}H NMR (300 MHz, $CDCl_3$): δ 8.756 (*s*, 4H), 4.360 (*t*, *J* = 6.75Hz, 2H), 4.206 (*t*, *J* = 7.5Hz, 2H), 2.697 (*t*, *J* = 6.3Hz, 2H), 2.363 (s, 6H), 1.735 (m, *J* = 4.425Hz, 2H), 1.475 (m, *J* = 7.44Hz, 2H), 0.994 (*t*, *J* = 7.35Hz, 3H).

2-(7-butyl-1,3,6,8-tetroxo-3,6,7,8-tetrahydrobenzo[lmn][3,8]phenanthrolin-2(1H)-yl-N,N,N-trimethylethan-1-aminium iodide (c)[S2]

b (0.1305g, 0.3 mmol) and methyl iodide (0.187g, 1.2 mmol) were dissolved in 80ml acetone at 56 ℃ for 3h until the appearance of purple precipitation. Then Purple solid was washed with $CHCl_3$ for several times to remove reactant and we collect the purple solid. (0.1069 g, 60.19% yield). ^{1}H NMR (300 MHz, DMSO): δ 8.711(*s*, 4H), 4.487 (*t*, *J* = 7.2Hz, 2H), 4.077 (*t*, *J* = 7.5Hz, 2H), 3.632 (*t*, *J* = 7.2Hz, 2H), 3.316 (s, 9H), 1.657 (*q*, *J* = 7.35Hz, 2H), 1.396 (*m*, *J* = 7.05Hz, 2H), 0.942 (*t*, *J* = 7.35Hz, 3H).

1.2.2. Synthesis of $(NDIA)_4Pb_3I_{10}$ crystal

NMP (3mL) solution of NDIA (0.075 mmol, 40 mg), PbI_2, (0.016 mmol, 7.8 mg) and 70 μL HI (55%, w/w) were added to a vial, EtOH was carefully added and layered on top of the vial. The vial was sealed put in the reaction kettle. The $(NDIA)_4Pb_3I_{10}$ crystal was obtained by programmed temperature controlling method. The temperature of the solution was decrease from 100 to 40 ℃ and then kept at 40 ℃ for more than two days. The crystalline $(NDIA)_4Pb_3I_{10}$ was successfully grown in the bottom of the reaction kettle after two days.

1.3.Crystallographic data collection and structure determination.

The SCXRD test was performed on a Saturn 724+ CCD diffractometer with Mo*Kα* irradiation (*λ* = 0.71073 Å) at *T* = 293 K. Data reduction was processed using CrystalClear software and the cell parameters were reduced and refined by the same one. The structures were solved and refined by Olex2-1.2.8 using ShelXS program *via* Direct Method to solve and ShelXL by least-squares method to refine. All non-hydrogen atoms were refined anisotropically. The crystal and refinement data are

summarized in Table S1, and selected bond distances and angles are shown in Table S2.

Table S1. Crystal data and structure refinement for $(NDIA)_4Pb_3I_{10}$.

Compound	**$(NDIA)_4Pb_3I_{10}$**
Crystal data	
Chemical formula	$I_{10}Pb_3 \cdot C_{21}H_{22}N_3O_4 \cdot C_{22}H_{25}N_3O_4 \cdot C_{21}H_{18}N_3O_4 \cdot C_{21}H_{23}N_3O_4$
M_r	3424.24
Crystal system, space group	Monoclinic, $P2_1/n$
Temperature (K)	293
a, b, c (Å)	12.882 (4), 61.295 (15), 16.037 (4)
β (°)	106.930 (4)
V (Å^3)	12114 (5)
Z	4
Radiation type	Mo $K\alpha$
μ (mm^{-1})	6.76
Crystal size (mm)	0.5 × 0.3 × 0.05
T_{min}, T_{max}	0.624, 1
No. of measured, independent and observed [$I > 2\sigma(I)$] reflections	47165, 18834, 13103
R_{int}	0.110
$(\sin \theta/\lambda)_{max}$ (Å^{-1})	0.597
Refinement	
$R[F^2 > 2\sigma(F^2)]$, $wR(F^2)$, S	0.095, 0.288, 1.04
No. of reflections	18834
No. of parameters	689
No. of restraints	305
H-atom treatment	H-atom parameters constrained
$\Delta\rho_{max}$, $\Delta\rho_{min}$ (e Å^{-3})	1.63, −1.87

Table S2. Selected bond distances and angles for $(NDIA)_4Pb_3I_{10}$.

Pb1—I4	3.3655 (14)	Pb2—I11	3.1276 (14)
Pb1—I7	3.2700 (15)	Pb2—I13^{ii}	3.3142 (14)
Pb1—I9	3.1037 (14)	Pb3—I4	3.2259 (14)
Pb1—I10	3.2736 (15)	Pb3—I5	3.2349 (14)
Pb1—I12	3.3025 (15)	Pb3—I6	3.2615 (15)
Pb1—I13	3.3018 (14)	Pb3—I7	3.1737 (15)
Pb2—I5	3.2054 (13)	Pb3—I8	3.2949 (14)
Pb2—I6	3.1770 (15)	Pb3—I12	3.2163 (14)
Pb2—I8	3.3558 (13)	I10—Pb2^{iii}	3.4015 (15)
Pb2—I10^{i}	3.4014 (15)	I13—Pb2^{iv}	3.3141 (14)
I7—Pb1—I4	84.16 (3)	I11—Pb2—I13^{ii}	97.66 (4)
I7—Pb1—I10	171.31 (4)	I13^{ii}—Pb2—I8	87.13 (4)
I7—Pb1—I12	81.66 (3)	I13^{ii}—Pb2—I10^{i}	101.67 (4)
I7—Pb1—I13	85.46 (3)	I4—Pb3—I5	177.74 (4)
I9—Pb1—I4	177.16 (4)	I4—Pb3—I6	96.21 (3)
I9—Pb1—I7	93.19 (4)	I4—Pb3—I8	95.42 (4)
I9—Pb1—I10	92.71 (4)	I5—Pb3—I6	83.88 (3)
I9—Pb1—I12	97.20 (4)	I5—Pb3—I8	86.83 (4)
I9—Pb1—I13	97.08 (4)	I6—Pb3—I8	80.63 (3)
I10—Pb1—I4	89.80 (3)	I7—Pb3—I4	88.05 (3)
I10—Pb1—I12	91.28 (4)	I7—Pb3—I5	91.95 (3)
I10—Pb1—I13	100.14 (4)	I7—Pb3—I6	175.17 (4)
I12—Pb1—I4	81.41 (4)	I7—Pb3—I8	96.75 (3)
I13—Pb1—I4	83.77 (4)	I7—Pb3—I12	84.52 (3)
I13—Pb1—I12	161.24 (4)	I12—Pb3—I4	84.92 (4)
I5—Pb2—I8	86.28 (4)	I12—Pb3—I5	92.83 (4)
I5—Pb2—I10^{i}	84.73 (4)	I12—Pb3—I6	98.08 (3)
I5—Pb2—I13^{ii}	170.86 (4)	I12—Pb3—I8	178.70 (4)
I6—Pb2—I5	85.73 (3)	Pb3—I4—Pb1	77.55 (3)
I6—Pb2—I8	80.93 (3)	Pb2—I5—Pb3	79.65 (3)
I6—Pb2—I10^{i}	167.61 (4)	Pb2—I6—Pb3	79.67 (3)
I6—Pb2—I13^{ii}	86.98 (4)	Pb3—I7—Pb1	79.69 (3)
I11—Pb2—I5	88.25 (4)	Pb3—I8—Pb2	76.65 (3)
I11—Pb2—I6	93.09 (4)	Pb1—I10—Pb2^{iii}	170.54 (5)
I11—Pb2—I8	172.17 (4)	Pb3—I12—Pb1	78.60 (3)
I11—Pb2—I10^{i}	94.50 (4)	Pb1—I13—Pb2^{iv}	172.07 (5)
Symmetry codes: (i) x+1, y, z; (ii) x+1/2, −y+1/2, z−1/2; (iii) x−1, y, z; (iv) x−1/2, −y+1/2, z+1/2.			

2. SEM image and EDX mapping of perovskite

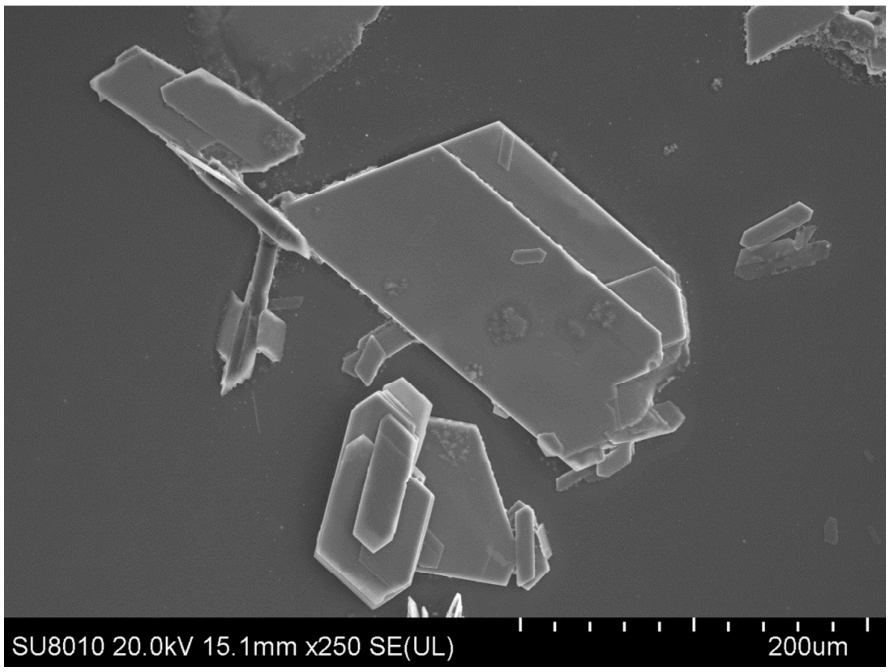

Figure. S1. SEM image of $(NDIA)Pb_3I_{10}$ crystal.

SEM and energy dispersive X-ray spectroscopy (EDS) mapping were used to examine the morphology and compositional distribution in the $(NDIA)_4Pb_3I_{10}$ crystalline plate. SEM observation clearly suggests the 2D layered plates with oblique hexagonal morphology. Some larger plates with size of tens to hundreds micron in length and width are observed. Each layer is tightly stacked to form a large lamellar structure. In Figure S2, distribution of all emblematic elements, including C, N, I and Pb, is observed, further confirming the formation of the perovskite structure.

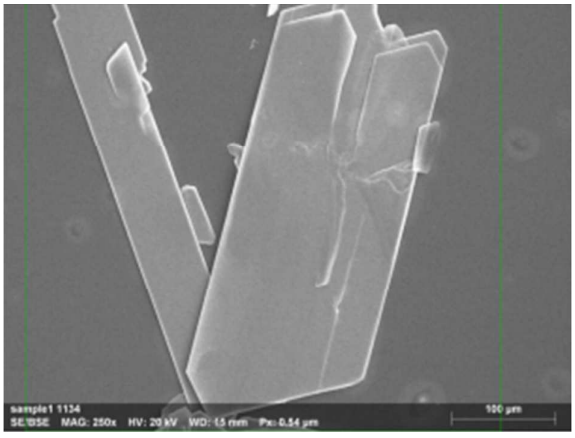

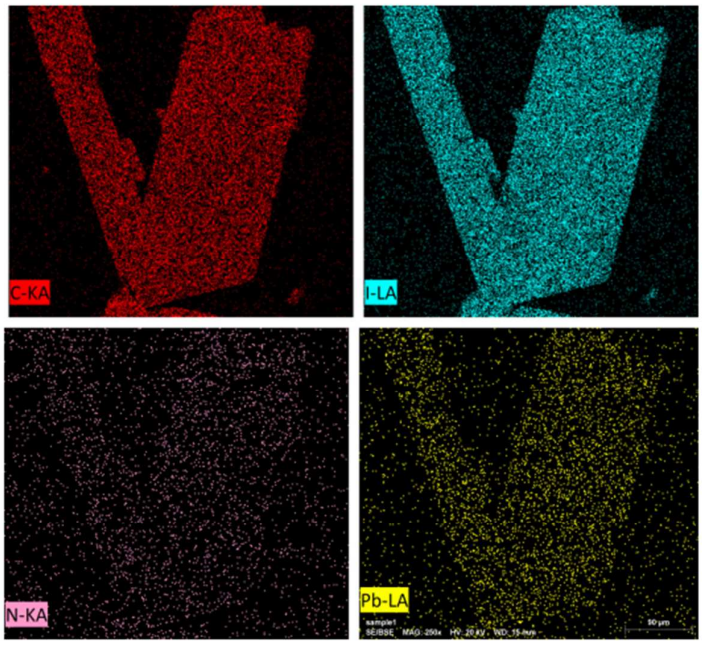

Figure S2. EDS mapping images of $(NDIA)_4Pb_3I_{10}$ crystals.

3. UV-vis absorption spectra and Tauc plots of UV−visible diffuse reflectance spectra.

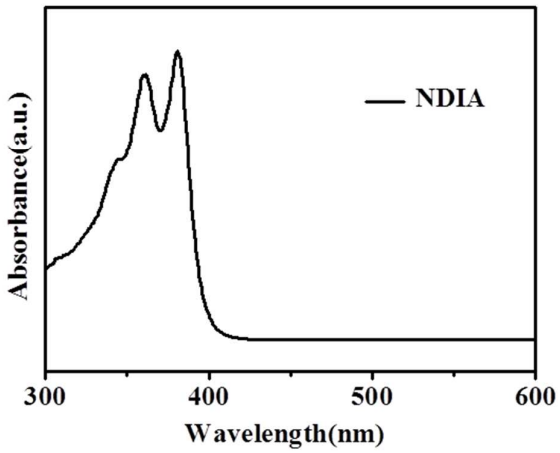

Figure S3. UV-vis absorption of NDIA in ethyl alcohol (1.2×10^{-5} mol L^{-1}).

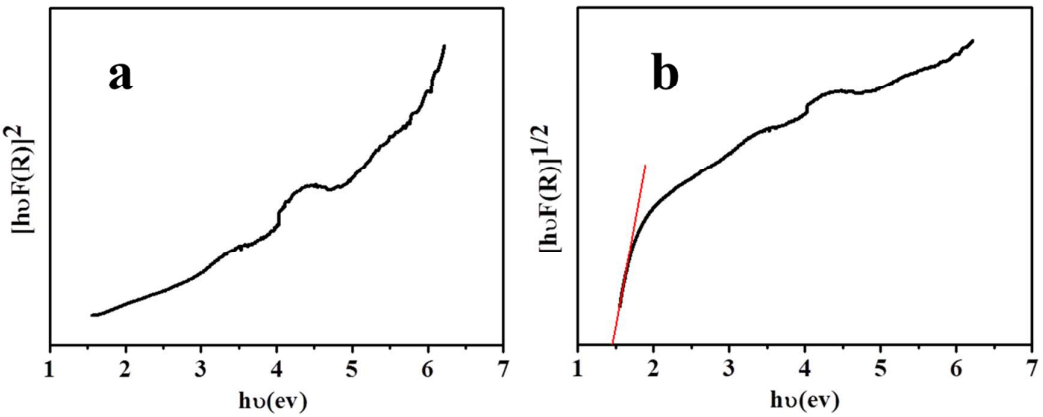

Figure S4. Tauc plots of UV−visible diffuse reflectance spectra used to determine the (a) direct optical gaps and (b) indirect optical gaps of $(NDIA)_4Pb_3I_{10}$ (diluted in $BaSO_4$).

4. X-ray Diffraction Analyses

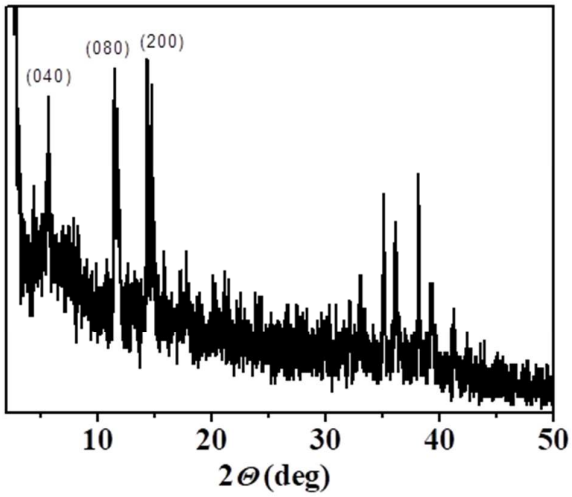

Figure S5. X-ray diffraction (XRD) patterns of the $(NDIA)_4Pb_3I_{10}$ crystalline plates.

5. AFM image

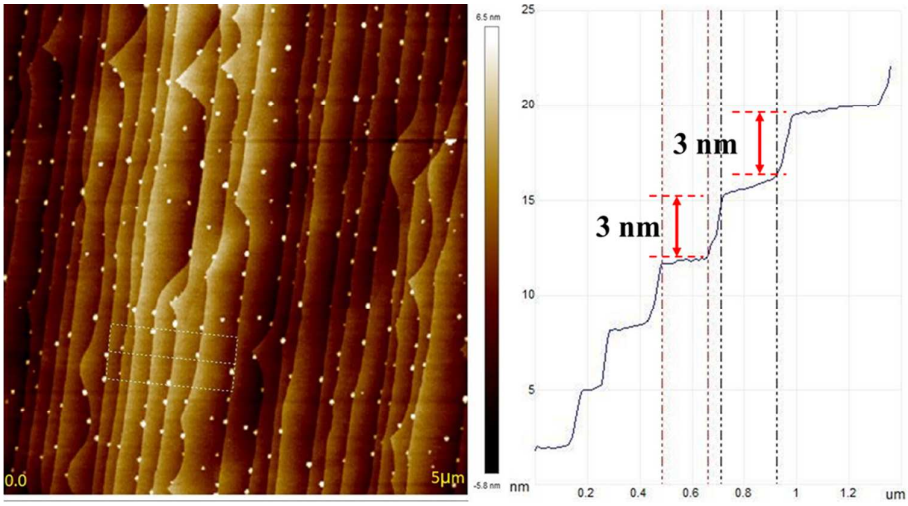

Figure S6. Tapping-mode AFM image of the surface of $(NDIA)_4Pb_3I_{10}$ crystal. Scale bar, 5μm. The interlayer thickness is about 3 nm, which is the half length of the unit cell in [010] direction.

6. BFDH simulation

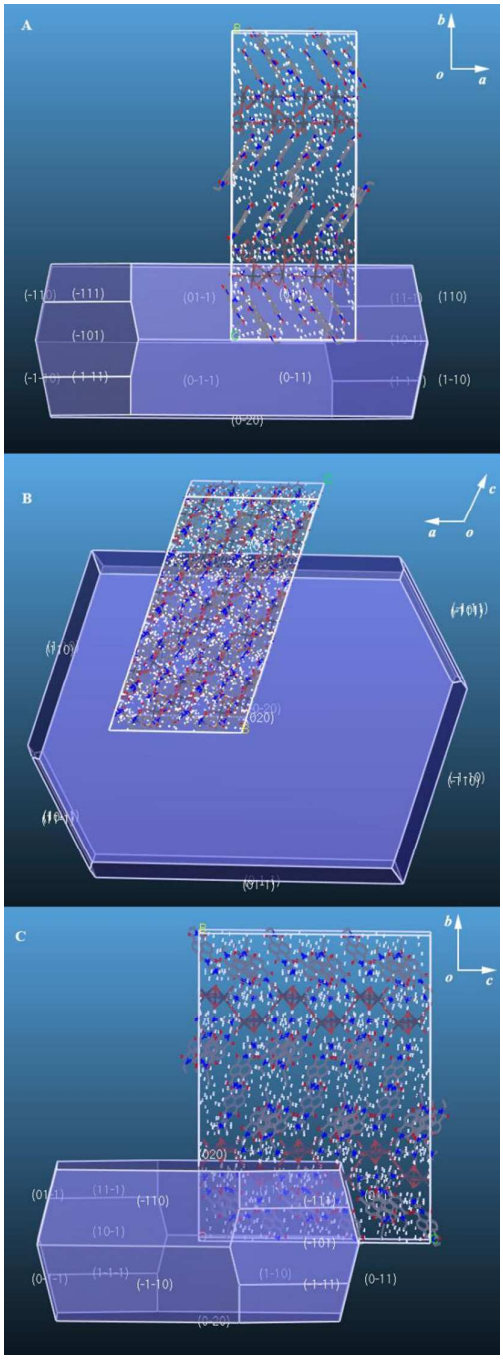

Figure S7. Theoretically predicted crystal habit (Bravais-Friedel-Donnay-Harker method, BFDH)[S3] of the single crystal $(NDIA)_4Pb_3I_{10}$: (A) along *c* axis; (B) along *b* axis; (C) along *a* axis.

7. Field Effect Transistors

7.1. Fabrication of the FET devices.[S4]

FET devices were fabricated in a top-contact and bottom-gate configuration. Heavily doped n-type Si wafer with 300 nm SiO_2 was used as the substrate. The substrate was cleaned sequentially in an ultrasonic bath with acetone, ethanol, and deionized water for 10 min each and then dried in the oven at 120 °C for 30 min. Later, the substrate surface was UV/ozone cleaned for 3 min and transferred to a N_2-filled glovebox. The polystyrene layer was coated onto the cleaned substrate via a spin-coating process at a spinning speed of 3000 rpm for 30s using a 4 mg/ml solution in toluene. Subsequently, the substrate was transferred to the oven to bake for 30 min at 80 °C in air. After that, the semiconductor layer of perovskite crysrtalline plate was transferred onto the substrate. Finally, Au with thickness of 100 nm was thermally evaporated (HHV, AUTO 306) through a shadow mask to form source and drain electrodes. Then template was removed with the forming of channel (L = 85 μm, and W depends on the crysrtalline plates).

7.2. Charge transport signature measurements.

All measurements were performed in air, using an Agilent B2902A Precision Source/Measure Unit in dark environment. The data were then analyzed with OriginPro software.

The field effect mobility, μ, was calculated according to the following equation:[S5]

$$\mu = \frac{L}{WC_i V_{DS}} \frac{\partial I_{DS}}{\partial V_G}$$

Where μ is mobility, C_i is the capacitance per unit area of the gate dielectric SiO_2 layer (300 nm, 1.15×10^{-8} F/cm^2). I_{DS} is source-drain current and V_G, V_{DS} is gate voltage and source-drain voltage, respectively. For FET devices, W and L represent the width and length of the single crystals crossing the source and drain electrodes, which are obtained from the microscopic observation.

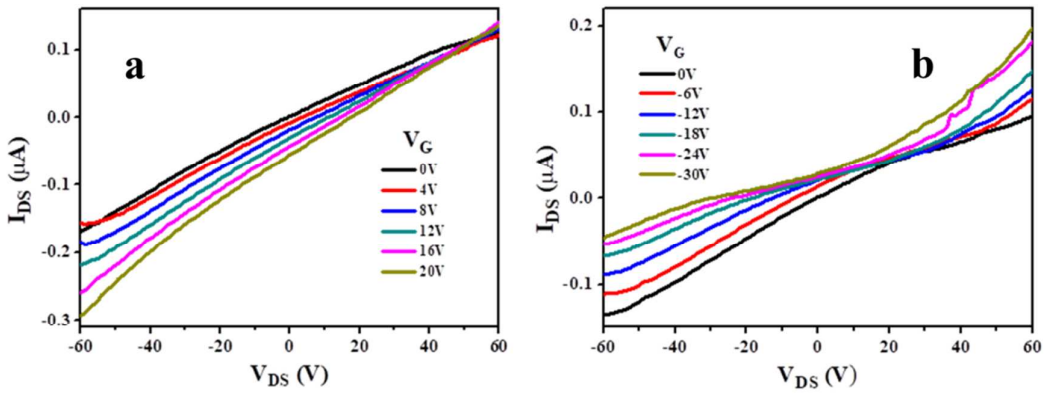

Figure S8. Output curves of an exemplary FET device based on $(NDIA)_4Pb_3I_{10}$ crystals at (a) V_G changed from 0 to 20V, and (b) V_G changed from 0 to -30V.

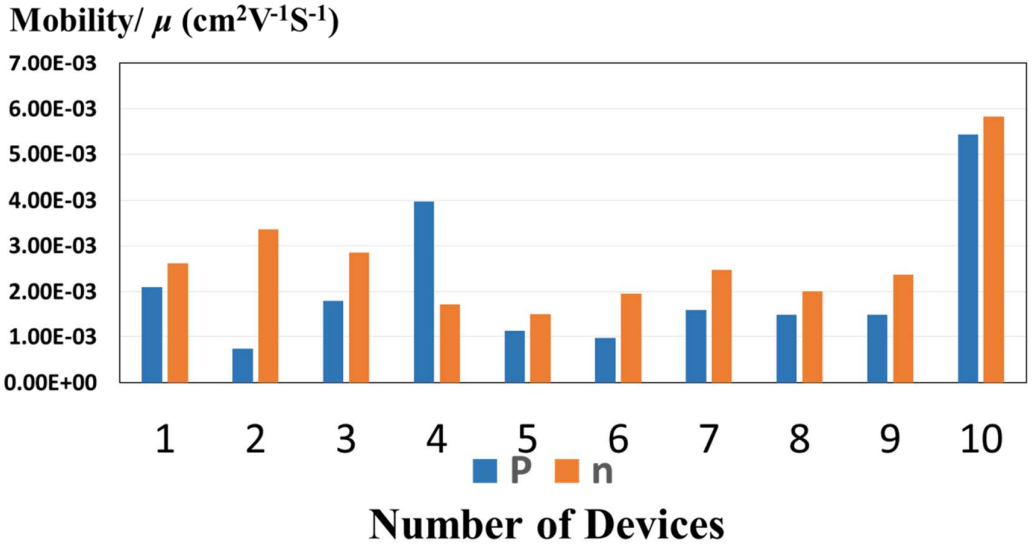

Figure S9. Carrier mobilities of 10 FET devices based on $(NDIA)_4Pb_3I_{10}$ crystals.

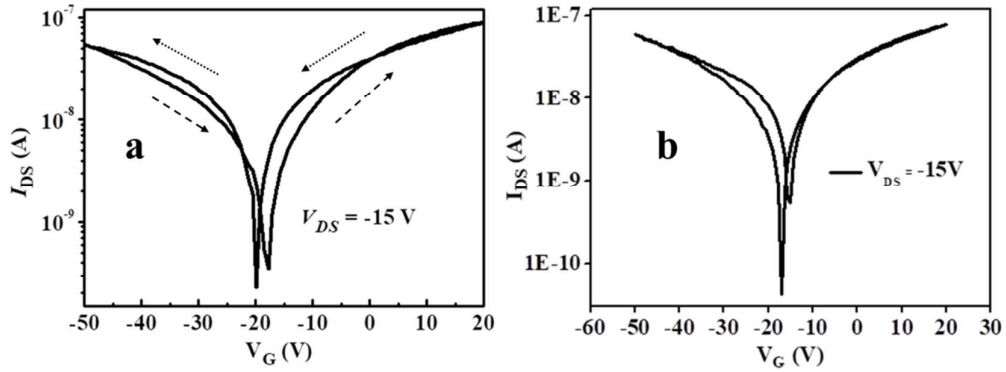

Figure S10. Hysteresis loops of (a) an exemplary FET device and (b) the same device stored in air for 7 days.

8. References

[S1] Zhou, D.; Wang, Y.; Jia, J.; Yu,W.; Qu, B.; Li, X.; Sun, X.; H-Bonding and Charging Mediated Aggregation and Emission for Fluorescence Turn-on Detection of Hydrazine Hydrate. *Chem. Commun.* **2015**, *51*, 10656.

[S2] Zhao, Y.; Li, X.; Aggregation Behavior of Naphthalimide Fluorescent Surfactants in Aqueous Solution. *Colloid Polym Sci.* **2014**, *292*, 687–698.

[S3] Jeffrey, M.; Orgiu, M. E.; Lieberwirth, I.; Pisula W.; Samorì, P. Charge Transport Over Multiple Length Scales in Supramolecular Fiber Transistors: Single Fiber Versus Ensemble Performance. *Adv. Mater.* **2014**, *26*, 430−435.

[S4] Ling, H.; Lin, J.; Yi, M.; Liu, B.; Li, W; Lin, Z.; Xie, L.; Bao, Y.; Guo, F.; Huang, W. Synergistic Effects of Self-Doped Nanostructures as Charge Trapping Elements in Organic Field Effect Transistor Memory. *ACS Appl. Mater. Interfaces.* **2016**, *8*, 18969–18977.

[S5] Li, D.; Cheng, H.-C.; Wang, Y.; Zhao, Z.; Wang, G.; Wu, H.; He, Q.; Huang, Y.; Duan, X. The Effect of Thermal Annealing on Charge Transport in Organolead Halide Perovskite Microplate Field-Effect Transistors. *Adv. Mater.* **2017**, *29*, 1601959.